PROCEEDINGS OF SCIENCE

IXPE - X-ray Polarimetry of Extended Sources: Supernova Remnants, Pulsar Wind Nebulae, the Galactic center...and more!

Riccardo Ferrazzoli[a,*] **and the IXPE Collaboration**[b]

[a] *INAF Istituto di Astrofisica e Planetologia Spaziali, Via del Fosso del Cavaliere 100, 00133 Roma, Italy*

[b] *https://ixpe.msfc.nasa.gov/partners_sci_team.html*

E-mail: riccardo.ferrazzoli@inaf.it

The NASA-ASI Imaging X-ray Polarimetry Explorer (IXPE) launched in December 2021 and has since enabled, for the first time, the ability to perform spatially resolved X-ray polarimetry in the 2 - 8 keV band for a wide range of extended sources. Thanks to its unique capabilities, IXPE has allowed us to probe the magnetic-field geometry closer than ever to the particle acceleration sites in young supernova remnant (SNR) shocks. It has also unveiled the level of magnetic turbulence and its distribution in pulsar wind nebulae (PWNe) and has even shed light on the recent past of our Galactic center (GC). Up to now, IXPE has observed six SNRs (Cas A, Tycho, SN 1006, RCW 86, RX J1713.7-3, and Vela Jr.), five PWNe (the Crab, Vela, MSH15-52, PSR B0540-69, and G21.5), the molecular clouds of the Sgr A complex near the GC, and the eastern lobe of the jet of the microquasar SS433. The X-ray polarimetric results from all the sources observed to date have exceeded, and in many cases subverted, our expectations. We present here the latest, unprecedented insights offered by the new field of spatially resolved X-ray polarimetry.

Frontier Research in Astrophysics – IV (FRAPWS2024)
9-14 September 2024
Mondello, Palermo, Italy

*Speaker

PoS(FRAPWS2024)044

1. Introduction

The NASA-ASI Imaging X-ray Polarimetry Explorer (IXPE) [1] is the first mission entirely dedicated to spatially resolved X-ray polarimetry. This is made possible by the capability of its instruments, the Gas Pixel Detectors (GPD)[2–4], which not only determine the photon impact position in their gas cell - enabling placement at the foci of X-ray optics for an angular resolution of $\sim$ 30" in the 2 - 8 keV energy band - but also track the resulting photoelectron's emission direction, thereby endowing IXPE with its polarization-measuring power. Hence, IXPE is uniquely equipped to observe and study extended sources such as Supernova Remnants (SNRs), Pulsar Wind Nebulae (PWNe), the molecular clouds in the Galactic center, and other exotic objects. For the first time, we can determine not only the X-ray polarimetric properties of these objects, but also how they change across different regions of interest. In Section 2 I will present the results obtained for the observation of SNRs, in Section 3 I will report on the PWNe observations. In Section 4 I will present the result for the observation of the extended jet of the microquasar SS433, and finally in Section 5 I will describe the IXPE observation of the molecular clouds in the Galactic center.

2. Supernova Remnants

Supernova remnants are the result of the violent death of a star whose ejected matter interacts with the interstellar medium and produces shocks. One of the major points of interest for the study of these objects is that their shocks are thought to be the dominant source of Galactic Cosmic Rays. In these shocks, particles are accelerated through the mechanism of diffusive shock acceleration (DSA, e.g. [5]) that requires strong and turbulent magnetic fields. The turbulence can be either preexisting or self-generated turbulence that can come from the streaming ions themselves. High resolution Chandra images found in these shocks X-rays emission from thin, ~few arcseconds, filaments that we ascribe to synchrotron emission. This means that a population of relativistic electrons must exist that is accelerated very close to the shocks, on spatial scales of $\sim 10^{17}$cm. Synchrotron radiation is intrinsically polarized, so even if IXPE, with its 30 arcseconds angular resolution, cannot resolve these filaments like Chandra does, we know that the X-rays and hence the polarized emission comes from close to the shocks. This is in contrast with, for example, radio-emitting electrons that instead traveled far from the acceleration regions. X-ray polarimetry allows us to determine the level of order of the magnetic fields and their orientation by measuring the degree of polarization and the polarization angle - that is orthogonal to its direction - respectively.
Indeed, the morphology of the magnetic field of SNRs is something we are very interested in because of a dichotomy that we observe in the radio band: old remnants tend to have tangential magnetic fields, whereas young SNR such as Cas A, or Tycho have radial magnetic fields. The reason for this difference is not yet known. One hypothesis argues for hydro-dynamical instabilities such as Rayleigh-Taylor filaments that are strung along and stretch out so that the magnetic field is carried along in those directions and the particles are spiraling along that magnetic field and that is what gives the radial orientation [6]. A second one calls for a sort of selection effect due to a more efficient particle acceleration in regions where the shock velocity is parallel to the magnetic field [7]. So the question is: why does this happen, and is it the same at smaller scales where X-rays are

emitted? As of now, IXPE observed six young SNRs: Cas A, Tycho, SN1006, RX J1713, RCW86, and Vela Jr, reporting results for all but the latter.

2.1 Cas A

Cas A was the first target of the IXPE scientific campaign after the launch and commissioning. It is a bright 350 years old remnant resulting from a core collapse explosion with its spectrum dominated by bright emission lines and by a non-thermal continuum [8, 9]. It also exhibits a clear reverse shock. The IXPE results were presented in [10]. A pixel-by-pixel search of the polarization signal, considering spatial bins of size 42" and 84" (see Fig. 1 (a)) revealed weak evidence for X-ray polarization of PD = 5 − 15%, and tangential PA, suggesting radial magnetic fields. In order to improve the sensitivity, circular symmetry of the polarization direction can be assumed, and exploiting the additivity of the Stokes parameters, larger emission regions could be combined. This method established highly significant detections of polarization from multiple regions: the forward shock, the forward shock plus a distinct region on the western edge of the reverse shock, and the whole remnant. This is illustrated in Fig. 1 (b) and (c) showing a three-color IXPE image of Cas A with these regions identified and their polarization plots of the most significative results, respectively. In the polarization plots, the PD is represented by the radial component of the polar plot, and the PA is measured relative to the radial direction. The contours show confidence intervals, and the pink circle illustrates the minimum detectable polarization at 99% confidence. The PA values for the forward shock (FS), the forward shock plus the western part of the reverse shock (FS+RSW), and for the whole remnant (All) are consistent with tangential polarization – and thus with radial magnetic fields – with PD values ranging from $\sim 2-4\%$. Correcting for the dilution due to the thermal flux, determined using Chandra spectral modeling of the regions of interest, the PD values of the X-ray synchrotron emission alone are no higher than $\sim 4\%$, that is, the value measured in the radio band. The low PD measured is suggestive of high levels of turbulence in the region close to the shock. The measured PA instead implies that that whatever the process that is responsible for the radial magnetic field observed in the radio, is already at work very close to the shock where particle are accelerated, on spatial scales corresponding to the thin rims ($\sim 10^{17}$ cm).

2.2 Tycho

The Tycho SNR is the result of a Ia explosion, observed as the historical supernova SN 1572 [11]. A fascinating peculiarity of Tycho are striking stripe-like synchrotron structures, highlighted by Chandra observations [12], whose origin is not yet well understood but theoretical studies suggested that they can be highly polarized [13–15]. Tycho was the second SNR observed by IXPE [16]. The analysis followed a similar approach to that used for Cas A, beginning with a pixel-by-pixel search for a signal. However, since Tycho is not as bright as Cas A, the polarization map binned on a 1 arcminute scale does not show highly significant detections (see Fig. 2 (a)). By aligning and summing over the data from different regions of interest, such as the highest significant region in the west, the rim, but also the whole remnant as shown in of Fig. 2 (b), highly significant detections of polarized emission were identified. The measured tangential PA corresponds to a radial magnetic field, consistent with the radio band polarization observations but originating from regions even closer to the shock. After accounting for the dilution by the thermal component, the X-ray PD in Tycho is significantly higher than for Cas A, $12\% \pm 2\%$ in the rim and $9\% \pm 2\%$ in

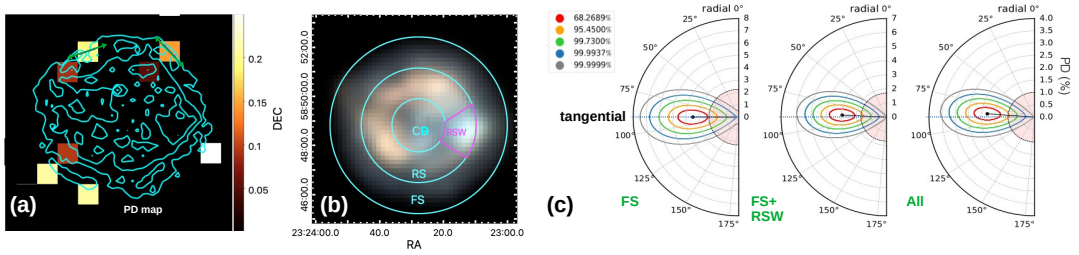

Figure 1: (a): Polarization map in the 3 - 6 keV energy band binned on a 42" pixel size of the SNR Cas A. Only pixels with confidence levels above 2σ are shown. For pixels with 3σ confidence level) the polarization angles are indicated with green arrows. **(b):** IXPE three color Stokes I image with superimposed the regions of interest used to test for an overall radial or tangential magnetic field orientation. The colder colors indicates a stronger non-thermal emission with respect to the warmer ones. **(c):** Polar diagrams of the measured PD and PA with respect to circular symmetry as confidence contours for the regions of panel **b**. The shaded pink region corresponds to the MDP99 level. Values around 90 degrees correspond to a tangentially oriented PA averaged over the region, while around 0∘ indicates on average a radially oriented PA. Images adapted from [10].

the whole remnant (see the polar plots in Fig. 2 (c) for the measured values in selected regions), suggesting maybe a lower turbulence level or longer turbulence scales.

2.3 SN 1006

The third remnant observed by IXPE was SN1006 [17]. Differently for the others, this one has a large angular extension, and indeed the IXPE field of view can cover only the northeastern limb of SN 1006. However, its spectrum is completely non-thermal [18], making it an ideal target for X-ray polarimetry. Compared to Cas A and Tycho, SN 1006 is significantly more extended, but fainter in the X-rays, hence background contributions from the source region were substantial, requiring their removal during analysis. IXPE resolved the double-rim structure of SN 1006 NE, enabling a detailed spatial analysis of the X-ray polarization. The Stokes I image of SN 1006 NE in the 2 – 4 keV range is shown in Fig. 3 (a), with the white and green regions indicating the shell and four sub-scale areas, respectively. The X-ray polarization of the entire shell was detected with a significance of 6.3σ, with PD = 22.4 ± 3.5% and PA = −45.5°, indicative of a radial magnetic field also in this case, and an even lower turbulence than the previous remnants. The sub-regions showed no significant variations of the polarization properties among them.

2.4 RX J1713.7-3946

RX J1713.7-3946 is a large (∼ 1 degree in diameter), entirely non-thermal [19, 20] shell-type SNR located in the Galactic plane. It is believed to have resulted from a Type Ib/c supernova, potentially linked to the historical SN 393 event [21–23], making it the oldest SNR whose results have been reported by IXPE to date [24]. IXPE observed the northwestern portion of this remnant. In Fig. 4 the binned and smoothed polarization map, the latter overlapped to the high-resolution Chandra image, and the polarization result for the whole NW shell are shown. Analysis of both the polarization map and regions of interest revealed that the polarization direction is perpendicular

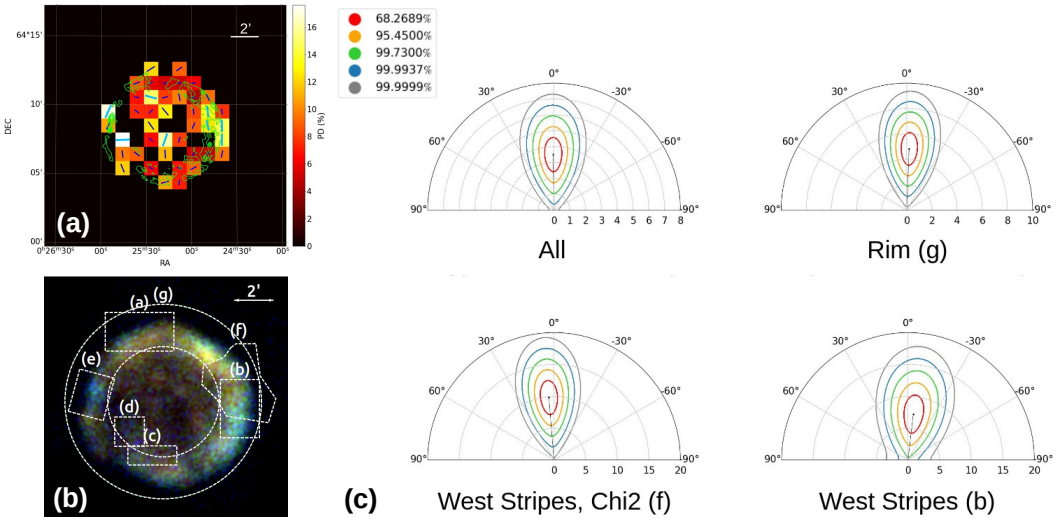

Figure 2: (a): Polarization map in the 3–6 keV energy band with a 1 arcminute pixel size. Only the pixels with significance higher than 1σ are shown. The blue bars represent the PA. The thicker cyan bars mark the pixels with significance higher than 2σ. Superimposed in green are the 4–6 keV Chandra contours. **(b):** IXPE three-color image of Tycho, superimposed are the regions of interest. **(c):** Polar plots for the most significative Tycho regions of interest. Values more consistent with a direction of polarization of 0 degrees correspond to an overall tangentially oriented polarization averaged over the region of interest. Images adapted from [16].

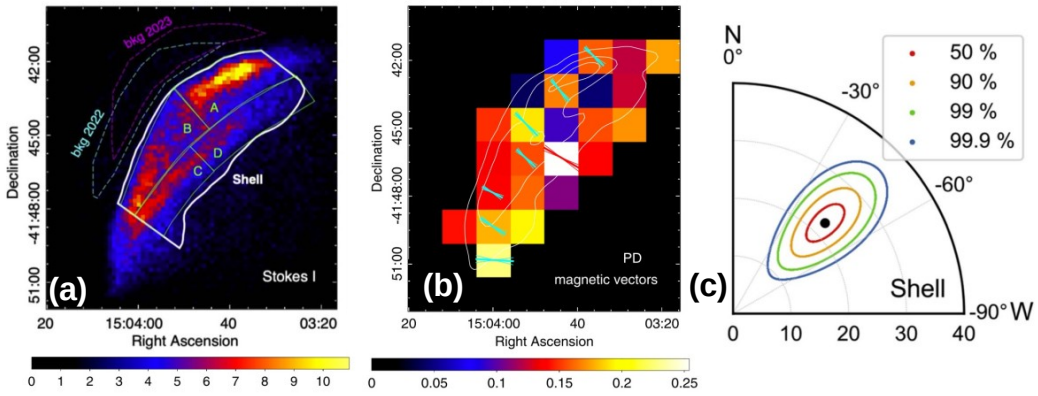

Figure 3: (a): IXPE Stokes I image in the 2–4 keV band of the SNR SN 1006 NW, with the regions of interest highlighted. The regions delineated with dashed lines correspond to the background regions. **(b):** PD map overlaid with magnetic field vectors and their 1σ uncertainties. The blue and red vectors correspond to pixels with significance $> 2\sigma$ and $> 3\sigma$, respectively. **(c):** polar plot of the Shell region after background subtraction. Images adapted from [17].

to the shock, with an average polarization degree of 12.5 ± 3.3% across the entire region. Unlike other IXPE-observed remnants, which exhibit radial magnetic fields, RX J1713.7-3946 is the first case where shock-compressed tangential magnetic fields dominate in the X-ray band. These results align with a model where shock compression of upstream isotropic turbulence generates a primarily tangential magnetic field.

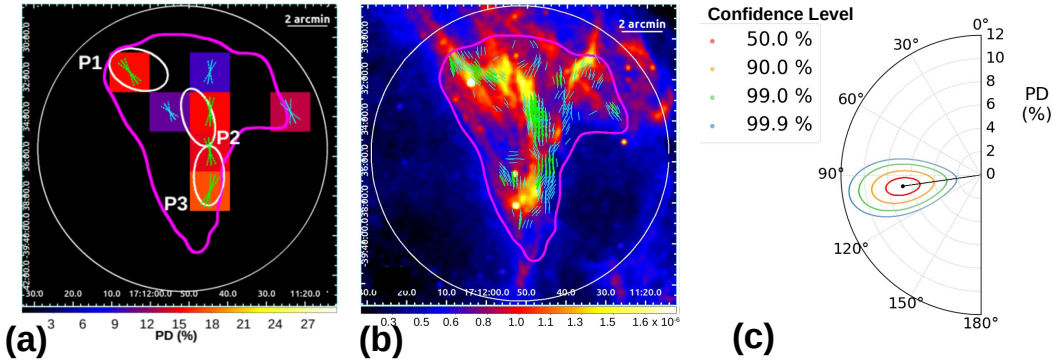

Figure 4: **(a):** polarization map binned with 2' wide pixels. The cyan and green vectors represent the direction of the magnetic field revealed at 2σ and 3σ significance levels, respectively. The length of the vectors is proportional to the PD. The dashed vectors show the 2σ uncertainty on the magnetic field direction in each pixel to improve the visibility. **(b):** Chandra exposure-corrected mosaic of 0.5-7 keV images of the northwest of RX J1713 with the IXPE field of view as a white circle, the IXPE 2-5 keV contours in magenta. In cyan and green, we show the magnetic field lines obtained through Gaussian smoothing of the IXPE data with $>2\sigma$ and $>3\sigma$, respectively. **(c)**: Polarization plot of the whole NW shell in the 2-5 keV energy band. Figures adapted from [24].

2.5 SNRs summary

According to the current picture of the X-ray polarimetry of SNR we have significant detection of polarization in four sources: Cas A, Tycho, SN1006, and RX J1713.7-3946. The former three have radial magnetic field, while the latter has a tangential one. The PD of the synchrotron emission ranges between 5% – 30%, pointing to high level of turbulence, as it is expected for efficient particle acceleration by DSA. The values vary between the SNRs, and there may be trends with the ambient density playing a role, or the Bhom factor (that is a measure of the acceleration efficiency). Whatever the case, new studies of Vela Jr, RCW 86, and the southwestern limb of SN 1006 will expand the parameter space. A recent study [25] suggested an explanation at least for the different morphology observed in the magnetic fields, that would depend on the relative sizes of the synchrotron emitting regions and the distance at which the radial component of the field peaks.

3. Pulsar Wind Nebulae

Pulsar wind nebulae (PWNe) produce X-ray emissions through the synchrotron process and are formed when plasma bubbles, accelerated to energies of 10–100 TeV, and magnetic fields generated

by a rapidly rotating neutron star, come into contact with the interstellar medium, encountering the surrounding supernova remnant or interstellar medium at a shock front. These interactions account for the intricate X-ray morphologies observed. PWNe are crucial environments for the detailed study of acceleration mechanisms and high-energy astrophysical phenomena. Utilizing X-ray polarimetry, we can investigate the location and level of magnetic field turbulence within the inner regions of the PWNe, areas marked by significant flaring and time variability, where high-energy particles are believed to be accelerated. This methodology enables us to differentiate between various theoretical models, including diffusive shock acceleration, reconnection, and turbulent acceleration [26–28]. Here, we briefly summarize the current IXPE findings of the most bright and extended among the published targets: the Crab nebula, the Vela PWN, and MSH 15-52.

3.1 Crab Nebula

The Crab Nebula is one of the most studied objects in the Universe, and the only one for which there was a significant detection of X-ray polarization before IXPE [29], but it was a single, spatially integrated measurement of the nebula that does not compare to the rich and diverse morphology that the high-resolution X-ray images show. IXPE observed the Crab Nebula three times for a total of 300 ks, with results reported by [30] and [31]. The results revealed a toroidal magnetic field (see Fig. 5) that extends beyond the brightest filaments, with a large level of asymmetry in the polarization degree, that goes as high as 45-50%, and is indicative of large variations in the amount of magnetic turbulence inside the PWN. The total space integrated PD is 20% with a PA of 145 degrees. While the PD is consistent between IXPE and OSO-8, the PA has a small but statistically significant difference from the 154 degrees measured by OSO-8. Such a difference could be due to changes in the morphology of the inner structure of the Crab Nebula. Measurements in the jet [31] suggest a change in the magnetic field flow from nearly perpendicular at the base to almost parallel at the end, maybe due to interaction with the surrounfing medium. Only one phase bin showed a polarization above the 3σ confidence level for the pulsar, at the center of the main peak, where the off-pulse subtracted emission gave a PD of $15.4 \pm 2.5\%$ and PA 105 ± 18 degrees.

3.2 Vela PWN

The Vela PWN was observed by IXPE with a total exposure of 860 ks and the results were reported in [32] (see Fig. 6). The PD was found to be remarkably high, reaching an image- and energy-averaged polarization degree of $\sim 45\%$, twice the value of the Crab Nebula. The PA was measured to be aligned to the axis of symmetry of the nebula ($\sim$ 50 degrees). From the spatially resolved image the polarization structure is toroidal and symmetric about the projected pulsar spin/proper motion axis. This symmetry is found to extend to even larger distances in radio polarization studies [33]. For some regions the PD can be as high as $\geq 60\%$, that is that is close to the maximum value allowed for synchrotron emission, implying that, across the emission region, the magnetic field is highly uniform and the electrons are accelerated in the PWN with almost no turbulence - differently from SNRs - challenging DSA scenarios and opening possibilities for other non-turbulent acceleration processes such as magnetic reconnection.

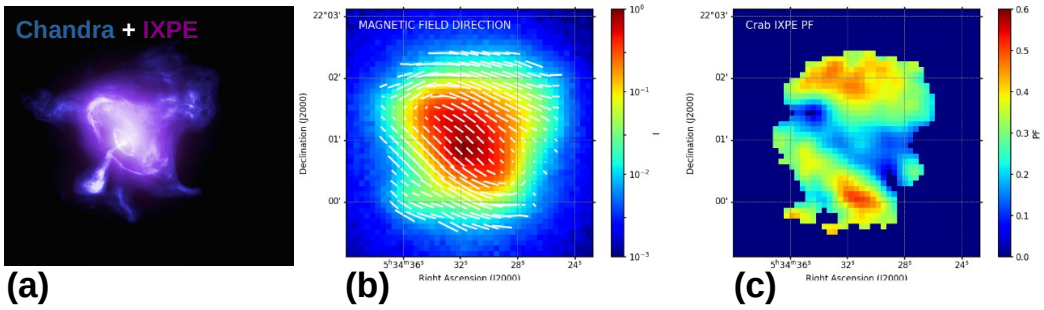

Figure 5: **(a):** Combined Chandra (blue) and IXPE (purple) images of the Crab Nebula. Credits: X-ray (IXPE: NASA), (Chandra: NASA/CXC/SAO) Image processing: NASA/CXC/SAO/K. Arcand & L. Frattare **(b):** total intensity map of the Crab Nebula in the 2 - 8 keV energy band, overlaid with the reconstructed magnetic field direction. **(c):** PD map cut above 5σ confidence level with the the gray dashed line indicating the nebular axis inferred from X-ray intensity maps. Images adapted from [30].

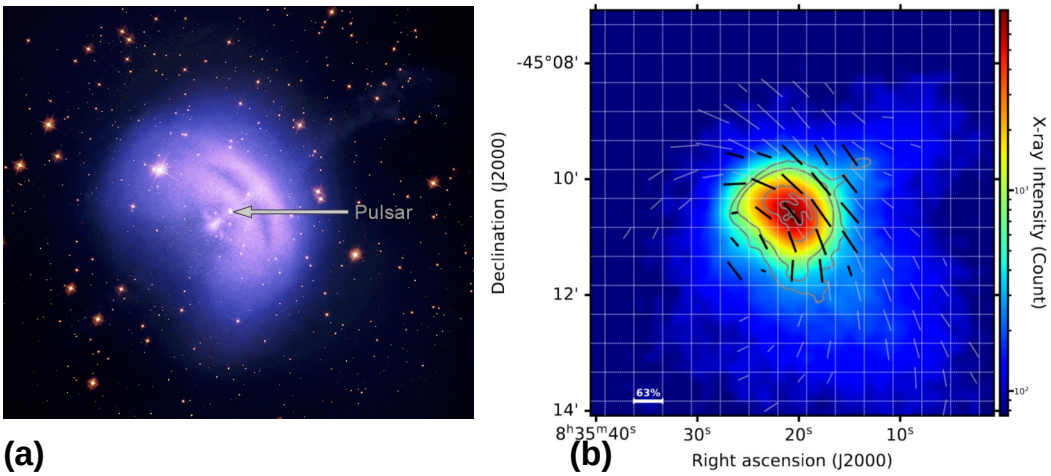

Figure 6: **(a):** Combined Chandra (blue), IXPE (purple), and Hubble images of the Vela PWN. The pulsar position is highlited. Credits, X-ray: (IXPE) NASA/MSFC/Fei Xie & (Chandra) NASA/CXC/SAO; Optical: NASA/STScI Hubble/Chandra processing by Judy Schmidt; Hubble/Chandra/IXPE processing & compositing by NASA/CXC/SAO/Kimberly Arcand & Nancy Wolk. **(b):** IXPE intensity map of the Vela PWN in the 2–8 keV range with the measured X-ray polarization (black lines) and radio polarization (grey lines) vectors overlaid. The grey contours comes from Chandra observations in the same 2–8 keV range. The bar at the bottom left presents the maximum measured X-ray PD of 63%. Adapted from [32]

3.3 MSH 15-52

MSH 15-52 is a spectacular $\sim 8'$ wide PWN, whose appearance in high-resolution Chandra images earned it the moniker of "Cosmic Hand". IXPE collected 1.5 Ms worth of data, with the results reported in [34]. IXPE mapped the the polarization across the arcs, jet, and finger regions, finding that the inferred magnetic field follows a complex pattern that wraps around the arc and the jet, and aligns with the linear fingers (see Fig. 7). Again, the polarization degree is very high and compatible with the synchrotron limit and reaching PD $\sim 70\%$ in several regions. This suggests that, similarly to Vela Jr, there are portions of the PWN containing uniform fields with little turbulence. Differently from the Crab and Vela, however, the toroidal component does not dominate the global field, likely because of the interaction between the SNR and the reverse shock.

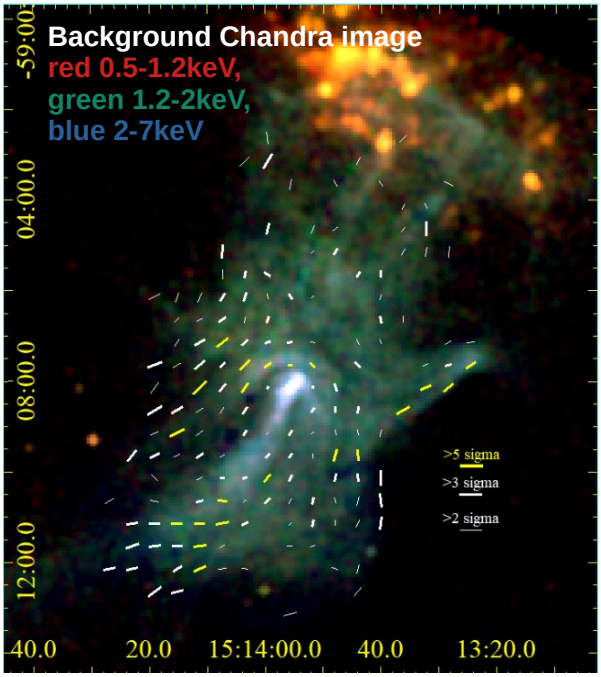

Figure 7: Energy-coded Chandra image of the PWN MSH 15-52 (red 0.5–1.2 keV, green 1.2–2 keV, blue 2–7 keV) with the magnetic field inferred by IXPE superposed: yellow bars show $>5\sigma$ polarization detections, thick white bars $>3\sigma$, and thin white bars $>2\sigma$. Image adapted from [34].

4. The eastern lobe of SS 433

A source that was not originally included in the IXPE observing plan, but that was added during the second year, is the Eastern lobe of the microquasar SS433. This system together with the extended remnant visible in the radio band is also known as the “Manatee Nebula”. This system is interesting for the question of how astrophysical systems translate the kinetic energy of the jet bulk motion into the acceleration of particles to very high energies, and the emission of TeV γ-rays from this source indicates the presence of high-energy particles. A region of hard X-ray emission in the

eastern lobe of SS 433 was recently identified with NuSTAR as an acceleration site, called "the head" [35]. IXPE targeted this region and observed it for ∼ 800 ks, measuring a PD in the range of 38% to 77% [36]. The high polarization degree indicates the magnetic field has a well ordered component if the X-rays are due to synchrotron emission. The PA is in the range -12 to +10 degrees (east of north) which indicates that the magnetic field is parallel to the jet (see Figure 8). Magnetic fields parallel to the bulk flow is similar to what has been also found in the jets of powerful radio galaxies. This may be caused by interaction of the flow with the ambient medium.

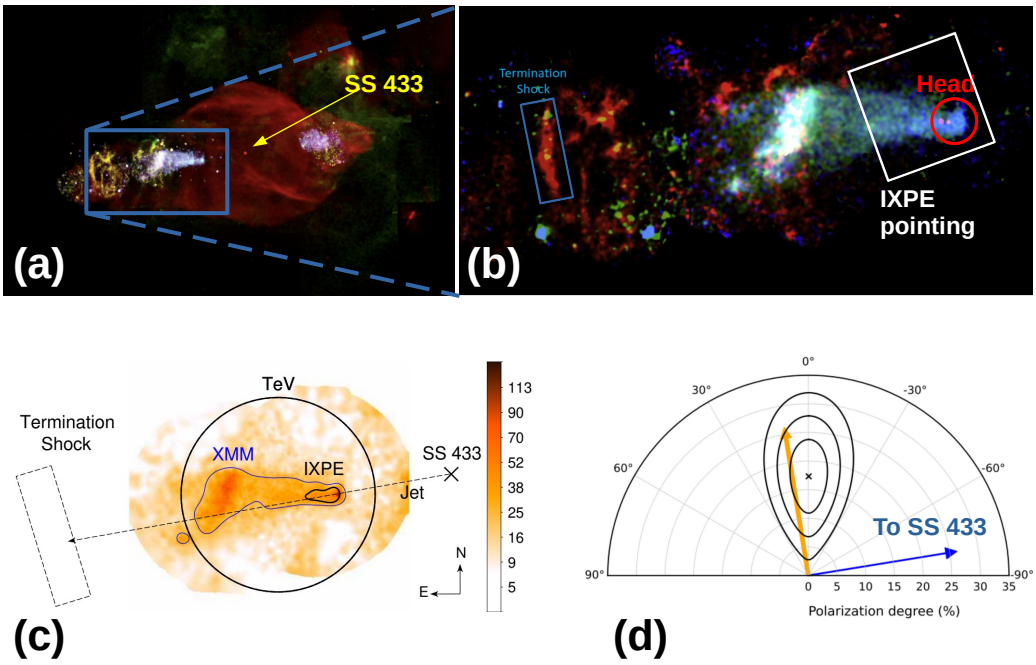

Figure 8: **(a):** Multiwavelength image of the Manatee Nebula hosting SS433 and **(b)** zoom on the eastern lobe with highlited the IXPE pointing. Images adapted from [35]. **(c):** XMM-Newton image in the 0.3–10 keV band, with the xmarking the position of SS433 and the dashed line indicating the jet axis. The dashed rectangle marks the jet termination shock, the blue contour the XMM-Newton image, the black contour is the IXPE source region, and the black circle is the region of the TeV gamma ray emission. **(d):** Contour plots of the polarization degree and angle. The × marks the measured value. The contours are at 68.27%, 95.45%, and 99.73% confidence intervals. The blue arrow indicates the direction from the lobe to the compact object while the orange arrow is the normal to it. Images adapted from [36].

5. The Galactic center

Last but not least, IXPE helped to investigate a mystery at the center of our Galaxy. Today we observe the SMBH at the center of the Milky Way, SgrA*, to be in a quiescent state and even dimmer than one would expect from a Black Hole of its mass. But we have hints, in the form of the Fermi and eRosita bubbles, that this may have not been always the case, at least on a timescale of millions of years. In the 300 light years region around it, many Molecular Clouds complexes like the ones

circled in the pictures, exhibit X-ray reflection features like a prominent Iron Kα line and a reflection continuum. However, no X-ray source strong enough to explain this X-ray reflection signature is currently present. The idea, first suggested by Sunyaev [37] is that the X-ray emission that we are seeing today is the light travel time-delayed echo of a strong activity by SgrA* some centuries ago, when it flared to be a million times brighter than today and more similar to a low luminosity AGN. There is then an obvious interest in the possibility of studying the recent history of SgrA* as a model for other SMBHs; and over the years many attempts have been made to reconstruct the past light-curve of Sgr A* using the X-ray spectral and morphological variability of these reflection nebulae. However, the distance along the line of sight of the clouds is poorly constrained, and this is a major source of uncertainty which makes difficult to infer the time-delay of the X-ray emission. An independent way to address this ambiguity is provided by X-ray polarimetry, as the reflected emission from a compact illuminating source is linearly polarized by scattering. The polarization angle is perpendicular to the scattering plane in which the direction of external illuminating source lies. This means that the detection of polarization from two or more sources allows to pinpoint the position of the source that in the past illuminated the molecular clouds. The polarization degree, instead, depends on the scattering angle, and so on the position of the cloud along the line of sight. So, an X-ray polarimetric measurement would not only identify the external source of illumination of the clouds, but also determine their distribution in the Galactic core [38, 39]. IXPE observed the Sgr A molecular cloud complex for 1 Ms [40], and a simultaneous Chandra observation identified the brightest clouds (see Fi. 9). Because of the low luminosity, high background, and contamination of the softer part of the spectrum by the unpolarized plasma permeating the region, in order to obtain a significant measurement we considered a large region encompassing the brightest features in the 4 – 8 keV band. IXPE found is a 2.8σ detection of PD of 31% ± 11%, and a polarization angle of $\sim$ 48 ± 11 degrees. The polarization angle is consistent with Sgr A* being the primary source of the emission, and the polarization degree implies that some 200 years ago, the X-ray luminosity of Sgr A* was briefly comparable to that of a Seyfert galaxy. In order to resolve the single clouds and determine the number and duration of the flares, we observed again this region for another Ms, and the analysis is currently ongoing.

5.1 A PWN-powered X-ray filament in the Galactic center: G0.13-0.11

The combined 2 Ms observation of the Galactic center has, however already yielded a serendipitous result [41]. IXPE discovered X-ray polarization from an X-ray bright filament called G0.13-0.11 in the Galactic Center region. This filament features a bright hard X-ray source, most plausibly a Pulsar Wind Nebula, and an extended and structured diffuse component. Combining, again, the polarization signal from IXPE with the imaging and spectroscopic data from Chandra, IXPE found that X-ray emission of G0.13-0.11 is highly polarized PD $\simeq$ 60% in the 3-6 keV band, while the polarization angle is perpendicular to the bright wings-like X-ray structure and to the nearby radio-emitting filaments, which are part of the GC Radio Arc. This high degree of polarization proves the synchrotron origin of the X-ray emission from G0.13-0.11. The magnetic field appears to be preferentially ordered along the filaments, and the PWN may power the larger radio arc behind it (see Fig. 10).

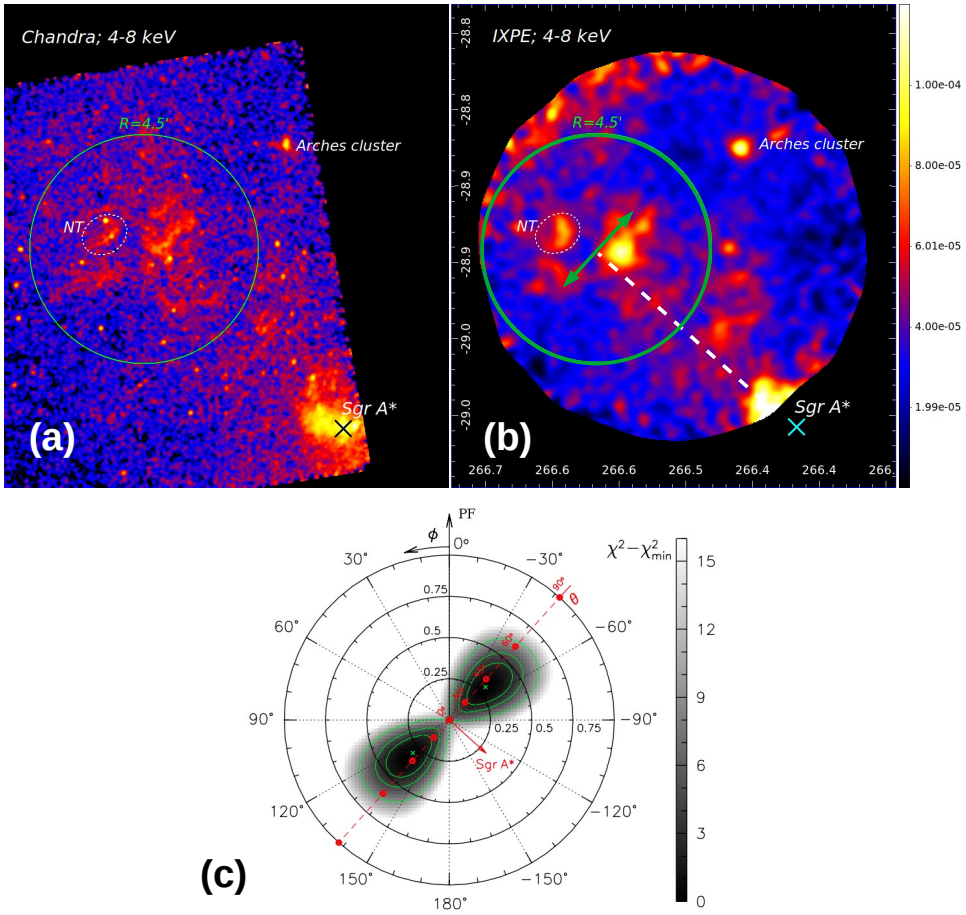

Figure 9: (a): Chandra 4–8-keV X-ray surface brightness maps of the Galactic Center region to the northeast of Sgr A*. **(b):** IXPE 4–8-keV X-ray surface brightness map. The positions of the supermassive black hole Sgr A* and the Arches star cluster are labeled. The area where reflection emission is strong in the Chandra data is shown using a green circle with a radius of 4.5'. The white dashed ellipse shows the location of the non-thermal source G0.13-0.11. The green arrow represent the best fit of the measured polarization direction, perpendicular to the direction of Sgr A* (dashed line). **(c):** polarization plot of emission from the green region in panels (a) and (b). The dashed red line marks the PA in the hypothesis that Sgr A* is the primary source of illuminating X-ray flux. The circles on this line depict expected PD for the scattering angle changing from 0 to 90 degrees. Figures adapted from [40].

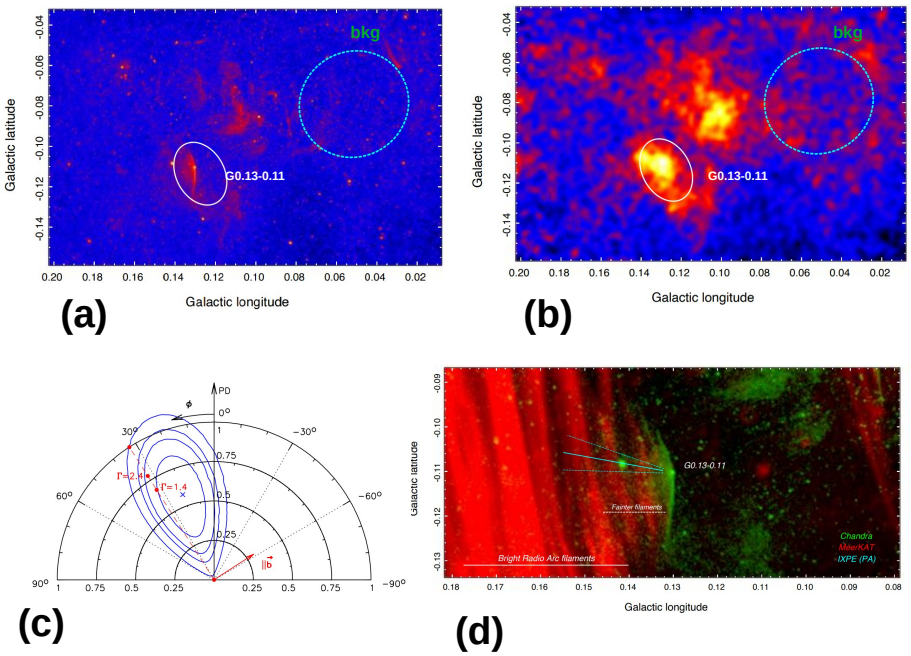

Figure 10: 3-6 keV Chandra **(a)** and IXPE **(b)** X-ray images. The white ellipse covers the G0.13-0.11 area, while the cyan region was used as a background extraction region. **(c):** polarization plot with the red dashed line illustrates the expected PA in the case, when the electric field vector is parallel to the Galactic plane, and two circles mark the maximum PD for synchrotron emission for different values of the spectral index. **(d):** Combination of radio (MeerKAT; 1.3 GHz, red) and X-ray (Chandra; 2.3-8 keV, green) images of G0.13-0.11. The cyan lines show the constraints on the PA measured by IXPE. Images adapted from [41].

6. Conclusions

The field of spatially resolved X-ray polarimetry has yielded incredible results, but it is not yet done: there are more results on the way from SNR, PWNe, form the Galactic Center, and hopefully even more unexpected results from one of the few classes of sources that have not yet been observed such as galaxy clusters.

Acknowledgments

The Imaging X-ray Polarimetry Explorer (IXPE) is a joint US and Italian mission. The US contribution is supported by the National Aeronautics and Space Administration (NASA) and led and managed by its Marshall Space Flight Center (MSFC), with industry partner Ball Aerospace (contract NNM15AA18C). The Italian contribution is supported by the Italian Space Agency (Agenzia Spaziale Italiana, ASI) through contract ASI-OHBI-2022-13-I.0, agreements ASI-INAF-2022-19-HH.0 and ASI-INFN-2017.13-H0, and its Space Science Data Center (SSDC) with agreements ASI-INAF-2022-14-HH.0 and ASI-INFN 2021-43-HH.0, and by the Istituto Nazionale di Astrofisica (INAF) and the Istituto Nazionale di Fisica Nucleare (INFN) in Italy. This research

used data products provided by the IXPE Team (MSFC, SSDC, INAF, and INFN) and distributed with additional software tools by the High-Energy Astrophysics Science Archive Research Center (HEASARC) at NASA Goddard Space Flight Center (GSFC). R.F. is partially supported by MAECI with grant CN24GR08 "GRBAXP: Guangxi-Rome Bilateral Agreement for X-ray Polarimetry in Astrophysics".

References

[1] Weisskopf, M., Soffitta, P., Baldini, L., Ramsey, B., O'Dell, S., Romani, R., Matt, G., Deininger, W., Baumgartner, W., Bellazzini, R., Costa, E., Kolodziejczak, J., Latronico, L., Marshall, H., Muleri, F., Bongiorno, S., Tennant, A., Bucciantini, N., Dovciak, M., Marin, F., Marscher, A., Poutanen, J., Slane, P., Turolla, R., Kalinowski, W., Di Marco, A., Fabiani, S., Minuti, M., La Monaca, F., Pinchera, M., Rankin, J., Sgro', C., Trois, A., Xie, F., Alexander, C., Allen, D., Amici, F., Andersen, J., Antonelli, A., Antoniak, S., Attinà, P., Barbanera, M., Bachetti, M., Baggett, R., Bladt, J., Brez, A., Bonino, R., Boree, C., Borotto, F., Breeding, S., Brienza, D., Bygott, H., Caporale, C., Cardelli, C., Carpentiero, R., Castellano, S., Castronuovo, M., Cavalli, L., Cavazzuti, E., Ceccanti, M., Centrone, M., Citraro, S., D'Amico, F., D'Alba, E., Di Gesu, L., Del Monte, E., Dietz, K., Di Lalla, N., Persio, G., Dolan, D., Donnarumma, I., Evangelista, Y., Ferrant, K., Ferrazzoli, R., Ferrie, M., Footdale, J., Forsyth, B., Foster, M., Garelick, B., Gunji, S., Gurnee, E., Head, M., Hibbard, G., Johnson, S., Kelly, E., Kilaru, K., Lefevre, C., Roy, S., Loffredo, P., Lorenzi, P., Lucchesi, L., Maddox, T., Magazzu, G., Maldera, S., Manfreda, A., Mangraviti, E., Marengo, M., Marrocchesi, A., Massaro, F., Mauger, D., McCracken, J., McEachen, M., Mize, R., Mereu, P., Mitchell, S., Mitsuishi, I., Morbidini, A., Mosti, F., Nasimi, H., Negri, B., Negro, M., Nguyen, T., Nitschke, I., Nuti, A., Onizuka, M., Oppedisano, C., Orsini, L., Osborne, D., Pacheco, R., Paggi, A., Painter, W., Pavelitz, S., Pentz, C., Piazzolla, R., Perri, M., Pesce-Rollins, M., Peterson, C., Pilia, M., Profeti, A., Puccetti, S., Ranganathan, J., Ratheesh, A., Reedy, L., Root, N., Rubini, A., Ruswick, S., Sanchez, J., Sarra, P., Santoli, F., Scalise, E., Sciortino, A., Schroeder, C., Seek, T., Sosdian, K., Spandre, G., Speegle, C., Tamagawa, T., Tardiola, M., Tobia, A., Thomas, N., Valerie, R., Vimercati, M., Walden, A., Weddendorf, B., Wedmore, J., Welch, D., Zanetti, D. & Zanetti, F. The Imaging X-Ray Polarimetry Explorer (IXPE): Pre-Launch. *Journal Of Astronomical Telescopes, Instruments, And Systems*. **8**, e026002 (2022,4)

[2] Costa, E., Soffitta, P., Bellazzini, R., Brez, A., Lumb, N. & Spandre, G. An efficient photoelectric X-ray polarimeter for the study of black holes and neutron stars. *Nature*. **411**, 662-665 (2001,6)

[3] Bellazzini, R., Angelini, F., Baldini, L., Bitti, F., Brez, A., Cavalca, F., Del Prete, M., Kuss, M., Latronico, L., Omodei, N., Pinchera, M., Massai, M., Minuti, M., Razzano, M., Sgro, C., Spandre, G., Tenze, A., Costa, E. & Soffitta, P. Gas pixel detectors for X-ray polarimetry applications. *Nuclear Instruments And Methods In Physics Research A*. **560**, 425-434 (2006,5)

[4] Soffitta, P., Baldini, L., Bellazzini, R., Costa, E., Latronico, L., Muleri, F., Del Monte, E., Fabiani, S., Minuti, M., Pinchera, M., Sgro', C., Spandre, G., Trois, A., Amici, F., Andersson,

H., Attina', P., Bachetti, M., Barbanera, M., Borotto, F., Brez, A., Brienza, D., Caporale, C., Cardelli, C., Carpentiero, R., Castellano, S., Castronuovo, M., Cavalli, L., Cavazzuti, E., Ceccanti, M., Centrone, M., Ciprini, S., Citraro, S., D'Amico, F., D'Alba, E., Di Cosimo, S., Di Lalla, N., Di Marco, A., Di Persio, G., Donnarumma, I., Evangelista, Y., Ferrazzoli, R., Hayato, A., Kitaguchi, T., La Monaca, F., Lefevre, C., Loffredo, P., Lorenzi, P., Lucchesi, L., Magazzu, C., Maldera, S., Manfreda, A., Mangraviti, E., Marengo, M., Matt, G., Mereu, P., Morbidini, A., Mosti, F., Nakano, T., Nasimi, H., Negri, B., Nenonen, S., Nuti, A., Orsini, L., Perri, M., Pesce-Rollins, M., Piazzolla, R., Pilia, M., Profeti, A., Puccetti, S., Rankin, J., Ratheesh, A., Rubini, A., Santoli, F., Sarra, P., Scalise, E., Sciortino, A., Tamagawa, T., Tardiola, M., Tobia, A., Vimercati, M. & Xie, F. The Instrument of the Imaging X-Ray Polarimetry Explorer. *Astrophys. J.*. **162**, e208 (2021,11)

[5] Malkov, M. & Drury, L. Nonlinear theory of diffusive acceleration of particles by shock waves. *Reports On Progress In Physics*. **64**, 429-481 (2001,4)

[6] Inoue, T., Shimoda, J., Ohira, Y. & Yamazaki, R. The Origin of Radially Aligned Magnetic Fields in Young Supernova Remnants. *Astrophys. J. Lett.*. **772**, eL20 (2013,8)

[7] West, J., Jaffe, T., Ferrand, G., Safi-Harb, S. & Gaensler, B. When Disorder Looks Like Order: A New Model to Explain Radial Magnetic Fields in Young Supernova Remnants. *Astrophys. J. Lett.* **849**, eL22 (2017,11)

[8] Reed, J.E.; Hester, J.J.; Fabian, A.C.; Winkler, P.F. The Three-dimensional Structure of the Cassiopeia A Supernova Remnant. I. The Spherical Shell. *Astrophys. J.* **1995**, *440*, 706.

[9] Vink, J.; Bloemen, H.; Kaastra, J.; Bleeker, J. The expansion of Cassiopeia A as seen in X-rays. *Astron. Astrophys.* **1998**, *339*, 201–207.

[10] Vink, J.; Prokhorov, D.; Ferrazzoli, R.; Slane, P.; Zhou, P.; Asakura, K.; Baldini, L.; Bucciantini, N.; Costa, E.; Di Marco, A.; et al. X-ray Polarization Detection of Cassiopeia A with IXPE. *Astrophys. J.* **2022**, *938*, 40.

[11] Green, D.; Stephenson, F. Historical Supernovae. *Supernovae Gamma-ray Bursters* **2003**, *598*, 7–19.

[12] Eriksen, K.; Hughes, J.; Badenes, C.; Fesen, R.; Ghavamian, P.; Moffett, D.; Plucinksy, P.; Rakowski, C.; Reynoso, E.; Slane, P. Evidence for Particle Acceleration to the Knee of the Cosmic Ray Spectrum in Tycho's Supernova Remnant. *Astrophys. J. Lett.* **2011**, *728*, eL28.

[13] Bykov, A.; Uvarov, Y.; Bloemen, J.; Den Herder, J.; Kaastra, J. A model of polarized X-ray emission from twinkling synchrotron supernova shells. *Mon. Not. R. Astron. Soc.* **2009**, *399*, 1119–1125.

[14] Bykov, A.; Ellison, D.; Osipov, S.; Pavlov, G.; Uvarov, Y. X-ray Stripes in Tycho's Supernova Remnant: Synchrotron Footprints of a Nonlinear Cosmic-ray-driven Instability. *Astrophys. J. Lett.* **2011**, *735*, eL40.

[15] Bykov, A.; Uvarov, Y.; Slane, P.; Ellison, D. Uncovering Magnetic Turbulence in Young Supernova Remnants with Polarized X-ray Imaging. *Astrophys. J.* **2020**, *899*, e142.

[16] Ferrazzoli, R.; Slane, P.; Prokhorov, D.; Zhou, P.; Vink, J.; Bucciantini, N.; Costa, E.; Di Lalla, N.; Di Marco, A.; Soffitta, P.; et al. X-ray Polarimetry Reveals the Magnetic-field Topology on Sub-parsec Scales in Tycho's Supernova Remnant. *Astrophys. J.* **2023**, *945*, e52.

[17] Zhou, P.; Prokhorov, D.; Ferrazzoli, R.; Yang, Y.-J.; Slane, P.; Vink, J.; Silvestri, S.; Bucciantini, N.; Reynoso, E.;Moffett, D.; et al. Magnetic Structures and Turbulence in SN 1006 Revealed with Imaging X-ray Polarimetry. *Astrophys. J.* **2023**, *957*, 55–69.

[18] Koyama, K.; Petre, R.; Gotthelf, E.V.; Hwang, U.; Matsuura, M.; Ozaki, M.; Holt, S.S. Evidence for shock acceleration of high-energy electrons in the supernova remnant SN1006. *Nature* **1995**, *378*, 255–258.

[19] Koyama, K.; Kinugasa, K.; Matsuzaki, K.; Nishiuchi, M.; Sugizaki, M.; Torii, K.; Yamauchi, S.; Aschenbach, B. Discovery of nonthermal X-rays from the Northwest Shell of the New SNR RX J1713.7-3946: The Second SN 1006? *Publ. Astron. Soc. Jpn.* **1997**, *49*, L7–L11.

[20] Slane, P.; Gaensler, B.; Dame, T.; Hughes, J.; Plucinsky, P.; Green, A. Nonthermal X-ray Emission from the Shell-Type Supernova Remnant G347.3-0.5. *Astrophys. J.* **1999**, *525*, 357–367.

[21] Wang, Z.; Qu, Q.; Chen, Y. Is RX J1713.7-3946 the remnant of the AD393 guest star? *Astron. Astrophys.* **1997**, *318*, L59–L61.

[22] Tsuji, N.; Uchiyama, Y. Expansion measurements of supernova remnant RX J1713.7-3946. *Publ. Astron. Soc. Jpn.* **2016**, *68*, e108.

[23] Acero, F.; Katsuda, S.; Ballet, J.; Petre, R. Measurement of the X-ray proper motion in the south-east rim of RX J1713.7-3946. *Astron. Astrophys.* **2017**, *597*, eA106.

[24] Ferrazzoli, R.; Prokhorov, D.; Bucciantini, N.; Slane, P.; Vink, J.; Cardillo, M.; Yang, Y.; Silvestri, S.; Zhou, P.; Costa, E.; et al. Discovery of a Shock-compressed Magnetic Field in the Northwestern Rim of the Young Supernova Remnant RX J1713.7-3946 with X-ray Polarimetry. *Astrophys. J. Lett.* **2024**, *967*, eL38.

[25] Bykov, A.M.; Osipov, S.M.; Uvarov, Y.A.; Ellison, D.C.; Slane, P. X-ray polarization: A view deep inside cosmic ray driven turbulence and particle acceleration in supernova remnants. *Phys. Rev. D* **2024**, *110*, 023041.

[26] Sironi, L. & Spitkovsky, A. Acceleration of Particles at the Termination Shock of a Relativistic Striped Wind. *Astrophys. J.*. **741**, e39 (2011,11)

[27] Zrake, J. & Arons, J. Turbulent Magnetic Relaxation in Pulsar Wind Nebulae. *Astrophys. J.*. **847**, e57 (2017,9)

[28] Takata, J. & Chang, H. Pulse Profiles, Spectra, and Polarization Characteristics of Nonthermal Emissions from the Crab-like Pulsars. *Astrophys. J.*. **670**, 677-692 (2007,11)

[29] Weisskopf, M., Silver, E., Kestenbaum, H., Long, K. & Novick, R. A precision measurement of the X-ray polarization of the Crab Nebula without pulsar contamination.. *Astrophys. J. Lett.* **220** pp. L117-L121 (1978,3)

[30] Bucciantini, N., Ferrazzoli, R., Bachetti, M., Rankin, J., Di Lalla, N., Sgrò, C., Omodei, N., Kitaguchi, T., Mizuno, T., Gunji, S., Watanabe, E., Baldini, L., Slane, P., Weisskopf, M., Romani, R., Possenti, A., Marshall, H., Silvestri, S., Pacciani, L., Negro, M., Muleri, F., De Oña Wilhelmi, E., Xie, F., Heyl, J., Pesce-Rollins, M., Wong, J., Pilia, M., et al. Simultaneous space and phase resolved X-ray polarimetry of the Crab pulsar and nebula. *Nature Astronomy*. **7** pp. 602-610 (2023,5)

[31] Wong, J., Mizuno, T., Bucciantini, N., Romani, R., Yang, Y., Liu, K., Deng, W., Goya, K., Xie, F., Pilia, M., Kaaret, P., Weisskopf, M., Silvestri, S., Ng, C., Chen, C., et al.. Analysis of Crab X-Ray Polarization Using Deeper Imaging X-Ray Polarimetry Explorer Observations. *Astrophys. J.*. **973**, e172 (2024,10)

[32] Xie, F., Di Marco, A., La Monaca, F., Liu, K., Muleri, F., Bucciantini, N., Romani, R., Costa, E., Rankin, J., Soffitta, P., Bachetti, M., Di Lalla, N., Fabiani, S., Ferrazzoli, R., Gunji, S., Latronico, L., Negro, M., Omodei, N., Pilia, M., Trois, A., Watanabe, E., et al. Vela pulsar wind nebula X-rays are polarized to near the synchrotron limit. *Nature*. **612**, 658-660 (2022,12)

[33] Dodson, R., Lewis, D., McConnell, D. & Deshpande, A. The radio nebula surrounding the Vela pulsar. *M.N.R.A.S.*. **343**, 116-124 (2003,7)

[34] Romani, R., Wong, J., Di Lalla, N., Omodei, N., Xie, F., Ng, C., Ferrazzoli, R., Di Marco, A., Bucciantini, N., Pilia, M., Slane, P., Weisskopf, M., Johnston, S., Burgay, M., Wei, D., Yang, Y., Zhang, S., et al. The Polarized Cosmic Hand: IXPE Observations of PSR B1509-58/MSH 15-5^2. *Astrophys. J.* **957**, e23 (2023,11)

[35] Safi-Harb, S., Mac Intyre, B., Zhang, S., Pope, I., Zhang, S., Saffold, N., Mori, K., Gotthelf, E., Aharonian, F., Band, M., Braun, C., Fang, K., Hailey, C., Nynka, M. & Rho, C. Hard X-Ray Emission from the Eastern Jet of SS 433 Powering the W50 "Manatee" Nebula: Evidence for Particle Reacceleration. *Astrophys. J.* **935**, e163 (2022,8)

[36] Kaaret, P., Ferrazzoli, R., Silvestri, S., Negro, M., Manfreda, A., Wu, K., Costa, E., Soffitta, P., Safi-Harb, S., Poutanen, J., Veledina, A., Di Marco, A., Slane, P., Bianchi, S., Ingram, A., Romani, R., Cibrario, N., Mac Intyre, B., Mikusincová, R., Ratheesh, A., Steiner, J., Svoboda, J., Tugliani, S., et al. X-Ray Polarization of the Eastern Lobe of SS 433. *Astrophys. J. Lett.* **961**, eL12 (2024,1)

[37] Sunyaev, R., Markevitch, M. & Pavlinsky, M. The Center of the Galaxy in the Recent Past: A View from GRANAT. *Astrophys. J.*. **407** pp. 606 (1993,4)

[38] Di Gesu, L., Ferrazzoli, R., Donnarumma, I., Soffitta, P., Costa, E., Muleri, F., Pesce-Rollins, M. & Marin, F. Prospects for IXPE and eXTP polarimetric archaeology of the reflection nebulae in the Galactic center. *Astronomy & Astrophysics*. **643** pp. eA52 (2020,11)

[39] Ferrazzoli, R., Di Gesu, L., Donnarumma, I., Soffitta, P., Costa, E., Muleri, F., Pesce-Rollins, M. & Marin, F. Prospects for a polarimetric mapping of the Sgr A molecular cloud complex with IXPE. *Astronomy & Astrophysics*. **655** pp. eA108 (2021,11)

[40] Marin, F., Churazov, E., Khabibullin, I., Ferrazzoli, R., Di Gesu, L., Barnouin, T., Di Marco, A., Middei, R., Vikhlinin, A., Costa, E., Soffitta, P., Muleri, F., Sunyaev, R., Forman, W., Kraft, R., Bianchi, S., Donnarumma, I., Petrucci, P., Enoto, T., et al. X-ray polarization evidence for a 200-year-old flare of Sgr A[*]. *Nature*. **619**, 41-45 (2023,7)

[41] Churazov, E., Khabibullin, I., Barnouin, T., Bucciantini, N., Costa, E., Di Gesu, L., Di Marco, A., Ferrazzoli, R., Forman, W., Kaaret, P., Kim, D., Kolodziejczak, J., Kraft, R., Marin, F., Matt, G., Negro, M., Romani, R., Silvestri, S., Soffitta, P., Sunyaev, R., Svoboda, J., Vikhlinin, A., Weisskopf, M., Xie, F., et al. Pulsar-wind-nebula-powered Galactic center X-ray filament G0.13-0.11. Proof of the synchrotron nature by IXPE. *Astronomy & Astrophysics*. **686** pp. eA14 (2024,6)

DISCUSSION

SILVIA ZANE: Do you think XRISM may be useful in discriminating between slow shocks and fast shocks in the two models?

RICCARDO FERRAZZOLI: maybe with XRISM we can have more precise measurements of line velocities, but here we are talking about large differences in velocity, so we don't need that kind of accuracy.

MANEL ERRANDO: Is there a leading hypothesis for why some SNRs show tangential B fields or radial? Does the fact that we are zooming in more into the shock region for large SNRs play a role?

RICCARDO FERRAZZOLI: A current idea proposed by Andrei Bykov is that the preferential direction of the X-ray polarization, and hence the magnetic field geometry, depends on the SNR physical parameters such as shock velocity and ambient density: a fast shock in a region with high enough density is a favorable place to produce tangential polarization of synchrotron radiation, that is, a dominantly radial turbulent magnetic field. The fact we are zooming in more into the shock region for large SNRs can't be the whole story, since for both SN 1006 and RX J1713 we are probing small linear scales, but we are seeing completely different behaviours.

ANDREA BELFIORE: In the maps you showed, what is the angular resolution?

RICCARDO FERRAZZOLI: The angular resolution for the IXPE detectors is $\sim$ 30". In the polarization maps it is useful to bin on different pixel scales in order to improve the statistics, at the cost of risking to mix regions with different polarization directions. It is hence important to reach an optimal trade-off between significance and correct physical representation.

DENYS MALYSHEV: How reasonable is to detect polarization from clusters of galaxies? To have polarization one needs synchrotron coming from relativistic electrons. The same electrons should also produce Inverse Compton in the GeV-TeV band. Currently no clusters are detected at GeV-TeV, so the level of synchrotron is minimal if not 0.

RICCARDO FERRAZZOLI: Indeed one might expect zero net polarization since galaxy clusters are roughly spherical and dominated by thermal emission. However, non-zero polarization may be produced by resonant scattering, enabling insight to the level of turbulence in the ICM, or by axion-like particles, which could provide important constraints on fundamental particle physics. Still, due to their low surface brightness, they would require long integration times.